Alternative techniques for casting process simulation

R.W. Lewis, R.S. Ransing, W.K.S. Pao, K. Kulasegaram and J. Bonet

Civil and Computational Engineering Centre, University of Wales Swansea, Swansea, UK

Received August 2002
Accepted January 2003

Keywords *Simulation, Optimization techniques, Finite element analysis*

Abstract *Over the past 20 years, casting process simulation has been an active area of research. The simulation techniques are either based on solving governing partial differential equations using numerical schemes such as the finite element or finite difference methods, or a variety of heuristically based geometry driven methods. Numerical methods are more accurate, but geometry driven methods are computationally less expensive. This paper explores two alternative techniques to overcome some of the limitations of traditional numerical simulation schemes for the casting process simulation. The first technique uses a geometric transformation method known as the medial axis transformation, to predict hot spots whereas the second technique, based on meshless methods, is used for simulating the mould filling process.*

1. Introduction

Casting is one of the oldest manufacturing processes. It is used widely in many industrial sectors and employs processes that are either gravity (e.g. die, sand and investment) or pressure fed. In all the cases, the purpose of the process is to produce near net shaped components. The design of the process must address the supply system for the molten metal, the feeding system as the part solidifies and shrinks and the thermal control to ensure the integrity of the cast component by the elimination of all forms of shrinkage porosity from within the casting. The volume of such a filling and feeding system needs to be minimised in order to ensure a high process yield. The cross-sectional area of the interface between the system and the cast component also needs to be minimised to reduce any fettling work.

Numerical simulation of the casting process has now become a mature field and a number of computational systems are available specifically for this purpose. In each case, following the analysis, there is a requirement to examine the results and to make a judgement on whether the system design is satisfactory or whether it needs to be improved in any way to ensure part integrity. Thus, the design of the process is an iterative procedure, based on trial and error technique. There is no certainty that an optimised design can be obtained under tight production schedules. The initial applications of

The authors would like to acknowledge the financial support given by EPSRC towards this research.

International Journal of Numerical Methods for Heat & Fluid Flow
Vol. 14 No. 2, 2004
pp. 145-166

0961-5539
DOI 10.1108/09615530410513782

numerical optimisation methods were in the structural optimisation domain where objective functions focussed on minimising weight or increasing the stiffness of the structure (Bletzinger *et al.*, 1992; Hinton *et al.*, 1992). By performing sensitivity analyses with respect to the design variables, it is possible to identify an optimised solution that minimises (or maximises) the objective function. One of the first investigations in the field of casting was reported by Lewis and Ransing (1998) and Morthland *et al.* (1995). This paper demonstrated the effectiveness of shape optimisation techniques to optimally design feeder volumes.

From discussion with experienced foundrymen, it was also realised that the accuracy of prediction is not a critical issue on many occasions. For a foundryman, the knowledge of a relative temperature profile and the locations of hot spots in a casting are important. It is also necessary for engineers to rerun a simulation overnight even for a slight change in the geometry. It is therefore advantageous to improve upon the computational speed by developing a useful, comprehensive and simple technique.

This paper is divided into the following three parts.

The first part will explore the use of medial axis transformation (MAT) for predicting temperature and hot spots in a casting process. MAT is a geometric reasoning tool, which stores the skeletal information of a solid. The technique has been shown to be useful in a wide variety of geometric reasoning applications ranging from design, interrogation, animation, finite element mesh generation, manufacturing simulation and detail suppression (Evans *et al.*, 1998; Gursoy and Patrikalakis, 1991; Sheehy *et al.*, 1996; Tam and Armstrong, 1991). The application of this technique for predicting cooling patterns in a solidifying metal is new. The paper also illustrates how the MAT can be used to predict thermal contraction. The advantage of using MAT is mainly in computational savings. The medial axis reduces the dimensionality of the problem by unity, e.g. the medial object of a three-dimensional object is a two-dimensional surface whereas the medial axis for a two-dimensional object is simply a curve. The saving in computational time becomes significant if the analysis is coupled with optimisation techniques. Finite element based optimisation techniques are inherently computationally expensive and hence the objective of this research is to develop techniques which can speed up the optimisation process without significant loss of accuracy.

The second part of this paper will focus on the finite element based optimisation techniques for designing optimal thermal control in a casting process. Two case studies have been presented.

The third section of the paper discusses another alternative technique for simulating the pressure die mould filling process. In this case, the objective of the research is not in saving computational time but to overcome the limitations of mesh-based methods in simulating jetting/splashing effects during mould filling. Mesh entanglement and distortion are the major

limitations of mesh-based methods. Meshless methods do not have these limitations and research is currently underway to explore the application of these techniques to simulate the mould-filling process.

2. Finite element based thermal models

The numerical analysis of thermal behaviour in a casting process is well-documented (Lewis *et al.*, 1997). The heat transfer between a casting and die/mould system is governed by conduction, whereas heat is removed from the system principally by convection from exposed exterior surfaces. The transient heat conduction equation is written as

$$\frac{\mathrm{d}H}{\mathrm{d}T}\frac{\mathrm{d}T}{\mathrm{d}t} = \nabla \cdot (k \nabla T) \tag{1}$$

For alloy systems, in simple models, the phase change is usually represented using an enthalpy method. More rigorous models are available and these make use of the phase diagram for the alloy system (Lewis *et al.*, 1997).

For a casting simulation process, the heat transfer between the cast and mould interface is influenced by the evolution of an air gap and/or the development of high contact stresses. The most convenient way of accounting for this is by means of an interface element in which the interfacial heat transfer is determined by means of a heat transfer coefficient h_i.

$$q = h_i(T_1 - T_2) \tag{2}$$

2.1 MAT and one-dimensional heat conduction

The MAT of a two-dimensional region was first introduced by Blum and Harry (1967) as an aid to the description of biological shapes. In two dimensions, the medial axis is a locus of the centre of an inscribed disc of maximal diameter as it rolls within the domain by maintaining the contact with the domain boundary. We notice that for a two-dimensional geometry, the MAT is a one-dimensional entity of the region. Some examples of the MAT for different shapes are shown in Figure 1.

The objective of this research is to explore the usage of MAT entities in obtaining approximate temperature solutions for a solidifying cast component using equations (1) and (2).

It was assumed that all the boundaries of the casting are homogeneous and that the heat flux emanates normally from the medial axes. This assumption is essentially one-dimensional and analytical solutions to such problems are given by Carslaw and Jaeger (2000). With the observation that the transient solutions are similar for a particular case of homogeneous boundary condition, the temperature values from the one-dimensional analytical solution are normalised with respect to the radius R of the largest inscribed circle and the maximum time t_0,

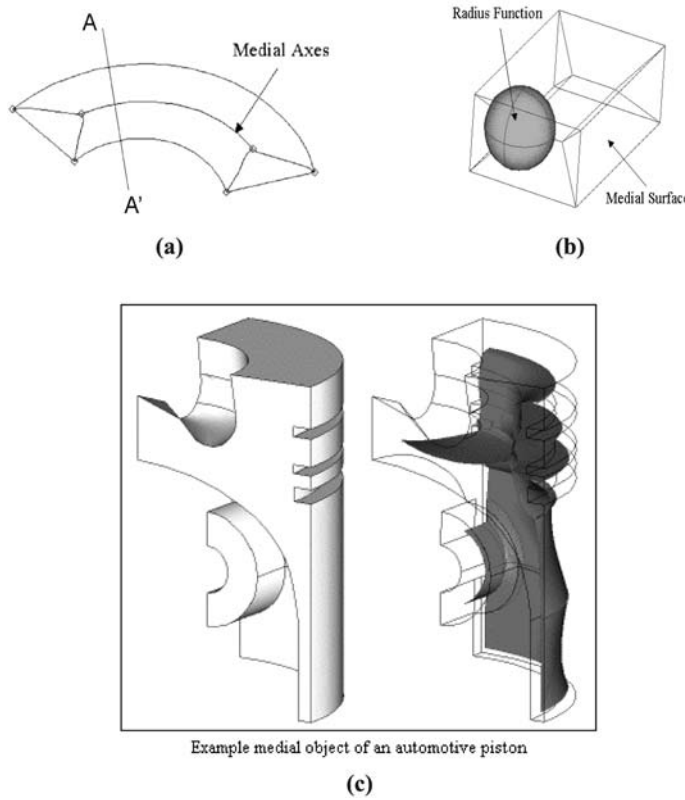

Figure 1.
(a) 2D object; (b) 3D object with their inscribed medial axes; and (c) 3D example of a medial object

$$T = T\left(\frac{d}{R}, \frac{t}{t_0}\right) \tag{3}$$

to obtain temperature values at any arbitrary point d, which is along a normal to the medial axis. With the knowledge of the location of the medial axes, together with the radial information of the inscribed circles at all junction points, the radius of the largest inscribed circle R can be determined. All coordinate points, d, perpendicular to the medial axes in the casting can now be normalised with respect to the maximum radius R. Thus, the transient temperature profile can be calculated by using equation (3) and a series of pre-determined one-dimensional transient analysis solutions (Pao *et al.*, 2002). Figure 2 schematically describes the procedure followed for the interpolation.

2.2 Numerical examples

In this section, we investigate the feasibility of the proposed medial axis interpolation method by comparing its solution with an equivalent finite element analysis. An L-shaped geometry, as shown in Figure 3, was selected as

a test case. Both arms of the L section have different thickness values so as to ensure that the method is capable of correctly interpolating the temperature profile under generalised geometry conditions. The initial temperature in the domain is 100°C, the ambient temperature is 25°C, $K = 1$, $\rho c = 1$, and $\alpha = 1$. The simulation was performed for a time span of 2.5 s, with a time step size of 0.1 s.

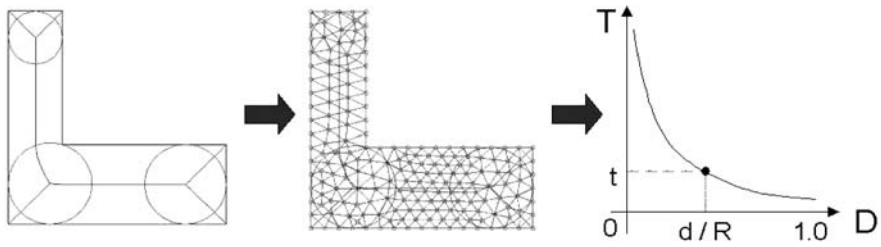

Figure 2.
Procedure for temperature interpolation

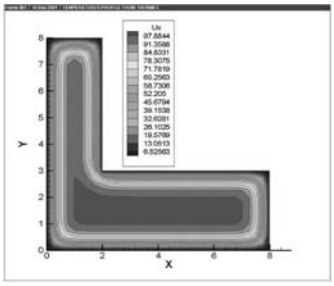

(a) 0.9 sec

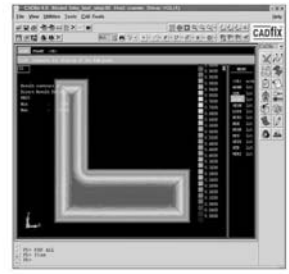

(b) 0.9 sec

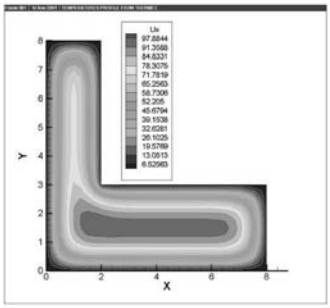

(c) 2.2 sec

Finite Element Simulation
(a and c)

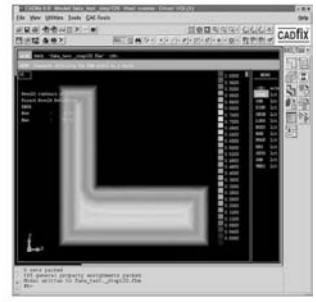

(d) 2.2 sec

Simulation using Medial Axis Transformation
(b and d)

Figure 3.
Comparison of finite element and interpolated temperature solution at different times

The temperature profiles at different time levels, obtained using the proposed method, are compared with the solution obtained by the finite element method (Figures 3(a)-(d)).

A realistic geometry has also been simulated with the same material properties and boundary conditions. Figure 4 shows the temperature distribution using the proposed technique at different time levels.

3. Thermal contraction simulation using MAT

In the foundry industry, experienced foundrymen would agree that the distorted shapes of the cast and moulded components can be predicted by using rules of thumb, visualising the skeletal geometry and identifying those sections of the geometry which solidify earlier in comparison with others. The distortion and shrinkage rules are applied to the representative skeleton of the geometry. For example, during solidification an "I" section will shrink along the vertical line and reduce in thickness. Similarly, shrinkage rules can be applied along the centrelines of U, L, V, O, H and T sections. It can be observed that these sections may be uniquely represented by a centreline if the thickness information is stored at every point along the centreline. The distortion and stress hotspots can then be identified by the selective application of shrinkage rules.

As described earlier, it can be observed that the scientific method to represent sections of the type L, U, I, etc. along the centreline is nothing but the geometry given by the MAT. A medial object stores all the necessary information about a given geometry so that it can be effectively used in any geometry-based reasoning technique. This section illustrates how this technique can be effectively used to predict thermal distortion. Figure 5 shows a solid material of height 1 m and width 0.6 m, together with its medial axes. The contours in this figure show the temperature difference that is applied as thermal loading over one-time step.

The temperature field is obtained by solving a steady-state heat conduction problem as described in a list of selected benchmarks published by Barlow and Davis (1986). This ensures that the prescribed temperature distribution is in no way an arbitrary choice, but are based on physically sound principles.

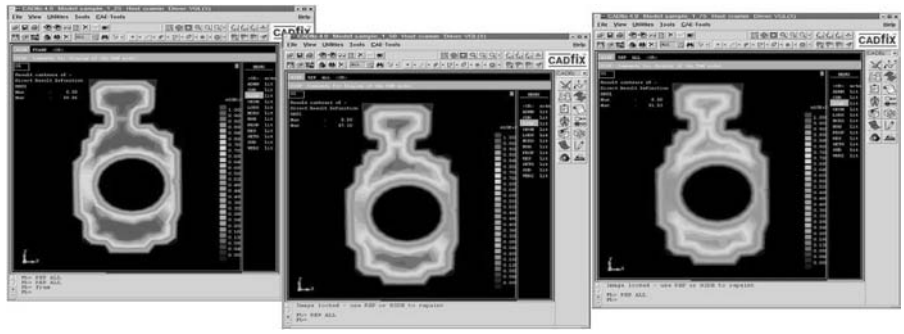

Figure 4.
Solidifying temperature profile in an arbitrary section at different time

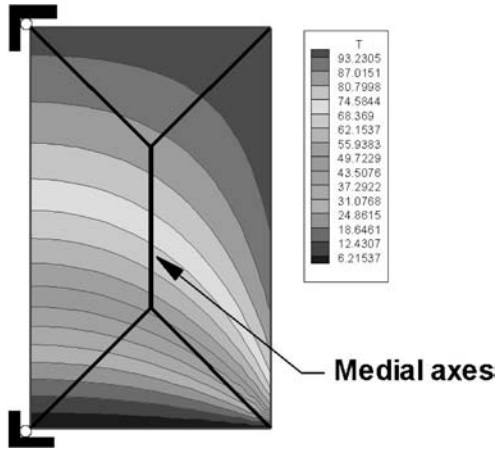

Figure 5.
Continuum test case with a thermal loading

On knowing the temperature distribution, the thermal contraction/expansion of the material can be solved by means of prescribing the thermal load to the quasi-static momentum balance equation (Chandrupatla and Belegundu, 1991) which is a standard FE procedure. At this stage, only an elastic model will be considered. The boundary conditions for the equilibrium problem are shown in Figure 5. The thermal expansion/contraction of the medial axes is modelled via beam elements. It is obvious that the beam model should have the same boundary conditions as the solid continuum model, i.e. a clamped boundary condition.

Figure 6 shows the comparison between the displacement profile for the continuum model and the beam model. It should be mentioned that the conventional Euler-Bernouli's beam model has been used for this

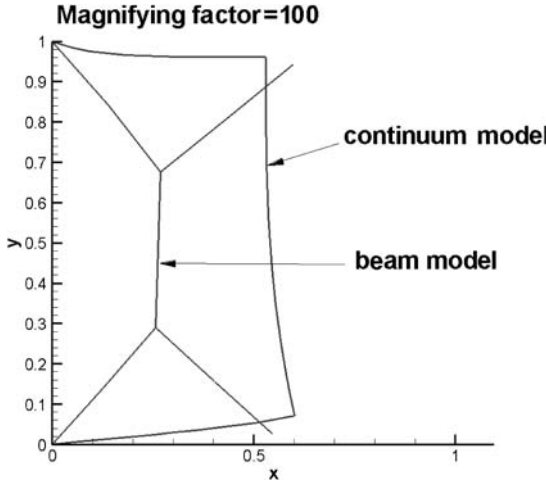

Figure 6.
Comparison between the continuum and beam displacements

analysis. The choice of this beam model is mainly due to its simplicity. In a specific thermal analysis for casting deformation, only the axial displacements are required, since a thermal loading essentially produces a hydrostatic state of stress. In the figure, displacements in both the X- and Y-directions have been magnified 100 times, and only the boundary of the deformed continuum model is shown. It is obvious that both the displacement profiles are *similar*, but the numerical values are not the same. The right upper arm of the beam moves further away while the right lower arm of the beam is less deformed as compared to the continuum solution. The reason for this discrepancy can perhaps be attributed to that fact that both right arms in the beams are free to move in both directions and are only constrained by their axial members. In the continuum model, the deformation of the right corner points is however constrained by their neighbouring points in both the X- and Y-directions. This research topic is still under investigation and it would appear that the inscribed circle radius information may need to be considered in a coupled way to achieve a better comparison.

4. Finite element based optimisation of casting processes

Numerical optimisation requires the definition of a design function. In the case of optimisation based on a heat transfer mechanism, this only needs to include variables that are affected by heat transfer, such as temperature or freezing time. In the case of shape optimisation the function needs to include dimensional (or mass) information as well as thermal contributions. It is usual to express this as an "objective function" that needs to be minimised or maximised. Also, the process design variables need to be maintained within the practical limits and this imposes constraints on the optimisation process. Thus, the optimisation process can be expressed mathematically as minimising (or maximising) the objective function $F(X)$, subject to the equality constraint

$$H_i(X) = 0 \quad i = 1, L \tag{4}$$

and the inequality constraint

$$G_j(X) \leq 0 \quad j = 1, M$$

In these equations, the variable X represents design variables, such as the heat transfer coefficient at the die wall or the dimensions of the feeding and filling system. The values L and M represent the number of constrained and unconstrained design variables. The optimisation process was carried out by means of the commercial code DOT (Vanderplaats, 1984). Following a sensitivity analysis, this evaluates the objective function and automatically perturbs the design variables so as to minimise (or maximise) the design function. In this work, the BFGS algorithm (DOT user manual, 1985) has been used due to its efficient convergence rate. The solution flow diagram for a finite element based optimisation algorithm is shown in Figure 7.

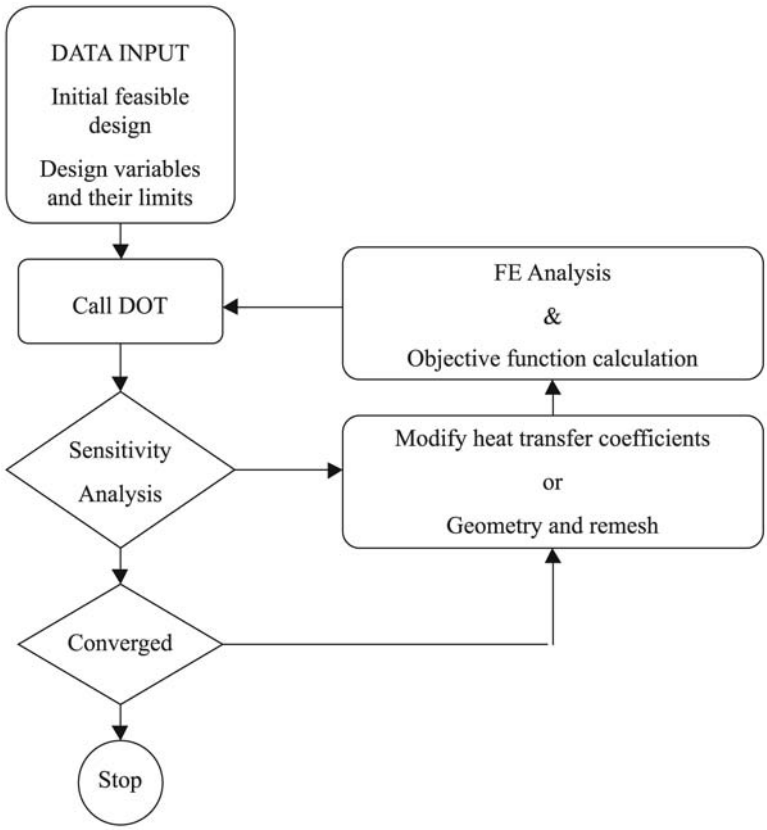

Figure 7.
Steps required in a finite element-based optimisation algorithm

Feeding design decisions such as the insulation around a feeder, provision of chills, exothermic pads or die coating thickness in the case of gravity dies, etc., are associated with an appropriate interfacial heat transfer coefficient value across the metal-mould interface. The objective of the feeding design is to keep the hot spots in the feeder, i.e. to eliminate the shrinkage porosity within a casting. The reliability of any numerical analysis, which is used to assist with this, largely depends on the heat transfer model used across the metal-mould interface.

4.1 Optimisation of temperature dependent interfacial heat transfer coefficients
This section describes a case study, which controls the interfacial heat transfer so as to achieve directional solidification to eliminate the occurrence of hot spots in a casting. In other words, if a hot spot is detected inside the casting then it is moved into the feeder.

The feed metal flow path is a path along which a feeder may feed the casting. For the casting example shown in this study (Figure 8), the feeder is expected to

feed the casting along the path from point 10 to 1. The user may input any desired feed metal flow path to the optimisation program.

If the feed metal has to flow along the path shown in Figure 8, then a freezing time gradient has to be maintained so that:

$$t_{f10} \rangle t_{f9} \rangle t_{f8} \rangle t_{f7} \rangle t_{f6} \rangle t_{f5} \rangle t_{f4} \rangle t_{f3} \rangle t_{f2} \rangle t_{f1} \tag{5}$$

where t_{fi} is the freezing time at point i. The freezing time at any point is defined as the time at which the temperature reaches the solidus temperature of the cast material. The nodal freezing times are calculated during the solidification analysis and from these values the freezing time at the ith design point can be interpolated by:

$$t_{f_{i\text{-node}}} = t - \Delta t \left[\frac{T^{t}_{i\text{-node}} - T_{\text{sol}}}{T^{t}_{i\text{-node}} - T^{t-\Delta t}_{i\text{-node}}} \right] \tag{6}$$

where $t_{f_{i\text{-node}}}$ is the freezing time at ith node, t the runtime, Δt the time step, $T^{t}_{i\text{-node}}$ the nodal temperature at time t, and T_{sol} the solidus temperature.

The objective function is then defined as a deviation from the defined feeder metal flow path:

$$\text{Cost} = n \sum_{i=1}^{s_n - 1} p \ \max\left[t_{f_i} - t_{f_{i+1}}, 0\right] \tag{7}$$

where n is the number of feed metal flow paths, s_n is the number of points in the nth feed metal flow path, p the penalty term, and t_{fi} is the freezing time at the ith design point.

The objective function states that if $t_{f_i} - t_{f_{i+1}}$ is negative, then the freezing time gradient is maintained and so the objective function is satisfied and assigned a zero value. If the gradient is not maintained, $t_{f_i} - t_{f_{i+1}}$ will be positive and this result is taken and then penalised. The penalty is

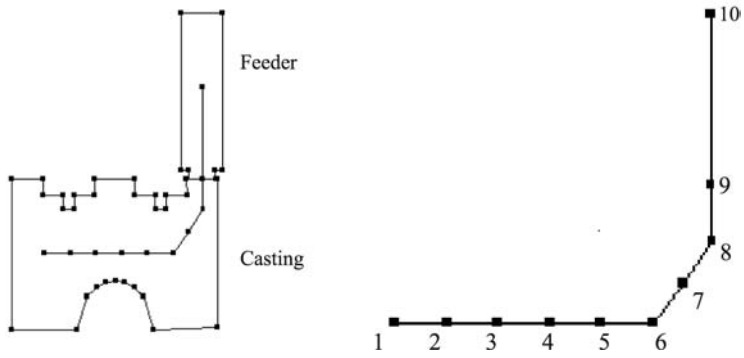

Figure 8.
An example of the feed metal flow path. Point 10 lies within the feeder and should solidify last

dependent on the distance from the farthest point from the feeder. The penalty increases with increasing distance from the farthest point.

The study uses a generalized equation proposed by Lewis and Ransing, (1998) that offers a natural choice for design variables, which can be used to optimise the die coating thickness. This definition of design variables allows us to consider the temporal variation of interfacial heat transfer coefficients (h), unlike the unrealistic heat transfer optimisation using constant interfacial heat transfer values, i.e.

$$h = \frac{e^{a_1} e^{-a_2/x^2}}{x^{a_3}} \quad \text{where} \quad x = \sqrt{2a_2/a_3} + \max(0, T_L - T_{int}) \tag{8}$$

where a_1, a_2 and a_3 are arbitrary constants with a range of 11-13.5, 100-1,000 and 1.0-1.2, respectively. T_L is the liquidus temperature and T_{int} is the casting interface temperature. The design variables are set as a_1, a_2 and a_3 at nine interface segments around the casting system (Figure 9).

Therefore, at each of the nine locations there are three variables a_1, a_2 and a_3, hence 27 design variables are used. These values have to be normalised in order to ensure that the optimisation effects of making changes to each variable is equal, since each variable is of a different magnitude. To do this the upper bound is assigned +1.0 and the lower bound is assigned as being -1.0.

The next stage of optimisation is the sensitivity analysis. A finite difference sensitivity method was used in this study. Each design variable was slightly perturbed individually while the others remained constant. A new value for the objective function was calculated using the gradient of the objective function with respect to the design variable. This was repeated for all design variables. A commercial software DOT (Vanderplaats, 1984) has been used for the sensitivity calculation and the subsequent optimisation.

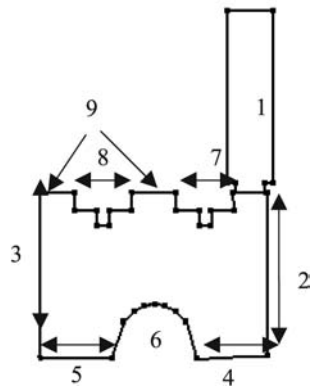

Figure 9.
Location of interface segments

$$\frac{\partial \text{Cost}}{\partial X_i} \approx \frac{\text{Cost}(X_1, X_2, \ldots, X_i + \Delta X_i, \ldots, X_n) - F(X_1, \ldots 4, X_n)}{\Delta X_i}$$
$$\frac{\partial G_j}{\partial X_i} \approx \frac{G_j(X_1, X_2, \ldots, X_i + \Delta X_i, \ldots, X_n) - G_j(X_1, \ldots, X_n)}{\Delta X_i} \quad (9)$$

4.1.1 Numerical simulation. The cast metal was an aluminium alloy LM25 with 615 and 550°C as liquidus and solidus temperatures, respectively. The mould was a steel mould with H13 material specification. The initial temperature for the melt and mould were assumed to be 625 and 150°C. The convection boundary condition of 75 W/m^2°C was applied on the outer surfaces and the ambient temperature was assumed to be 25°C. Constant conductivity values of 186.3 and 33.9 W/m°C and density 2,790 and 7,721 kg/m^3 were assumed for the metal and mould, respectively. The temperature dependent enthalpy curve used has been tabulated (Table I).

The interfacial heat transfer coefficient variation, as shown in Figure 10, was input to the optimisation program. The corresponding freezing time contours are shown in Figure 11. The optimal freezing time contours are shown in Figure 12 with corresponding interfacial heat transfer variations as shown in Figure 13. It has been recommended that locations 3 and 6 be cooled fastest with a starting interfacial heat transfer value of around 8 kW/m^2°C. Locations 5 and 8 have a starting value in a similar range of 5.5 kW/m^2°C. Insulation has been proposed for locations 1 and 2 (with a starting value of 450 kW/m^2°C). Feeding design decisions, such as insulation around a feeder, provision of

Table 1. Enthalpy curve used for the metal and mould

Metal		Mould	
Temperature (°C)	Enthalpy (J/kg)	Temperature (°C)	Enthalpy (J/kg)
0	0	0	0
550	6.011×10^5	200	1.424×10^5
615	1.0699×10^6	400	2.488×10^5
800	1.2721×10^6	800	5.696×10^5

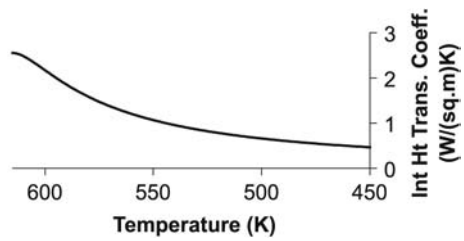

Figure 10. Initial heat transfer coefficient variation (same at all interface locations)

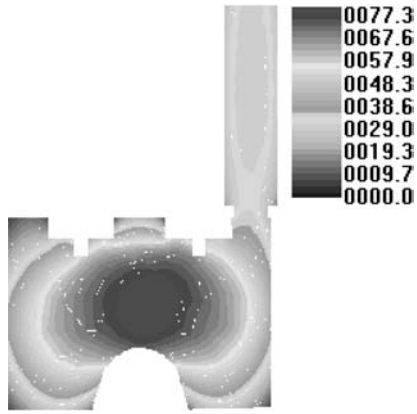

Figure 11.
Initial freezing time contours

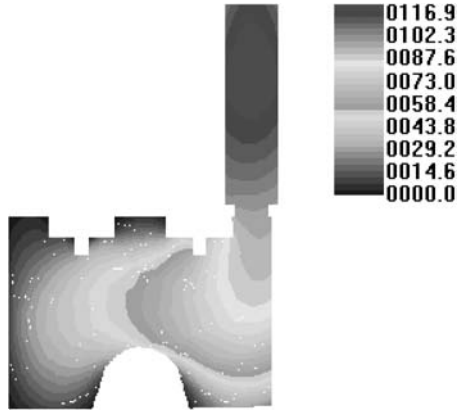

Figure 12.
Optimal freezing time contours

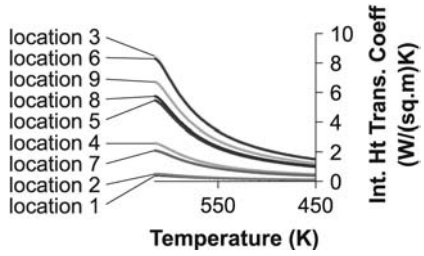

Figure 13.
Final temporal variation of heat transfer coefficients at various locations

chills, exothermic pads or die coating thickness in the case of gravity dies, etc., are associated with an appropriate interfacial heat transfer coefficient value across the metal-mould interface and may be designed according to these predictions.

4.2 Shape optimisation of feeders

The second case study is shown in Figure 14. This comprises a simple aluminium hub that is cast by means of the gravity die process and uses LM25 as the alloy material. In this case, the aim is to optimise the size of the feeding system that is positioned on top of the casting.

Since this part is also bottom filled through a small section, again it will be assumed that the filling system does not contribute to this phase of the process, even though the filling cup represents a large volume of metal in the die. Figure 14 shows only the cast part and top feeder system. The potential shape changes that will be available to optimise the shape of the feeding system are also shown in the figure. This allows changes in feeder size as well as the sectional area that links with the cast part itself. In this case, the objective function must include both the thermal and volume components. It is now given by:

$$F(X) = \{T_A - T_B + C\} + W\left\{\frac{\text{Volume of Feeder}}{\text{Max. Volume of Feeder}}\right\} \tag{10}$$

where T_A and T_B are the temperatures at points A and B at 500 s; C is the forces at the thermal gradient, here $C = 20$; and W is the weighing of the shape optimisation, here $W = 1$.

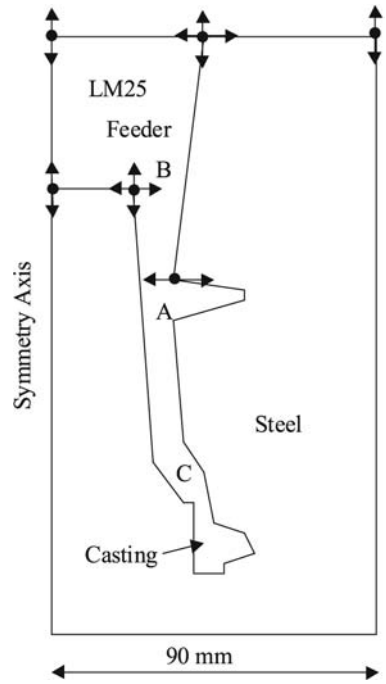

Figure 14.
Schematic view of the hub casting and feeding system

This choice of function ensures the directional solidification of the part via the thermal contribution and the effect of the feeder size and shape by means of the mass term.

The calculations were carried out for an ambient temperature value of 25°C with a convective heat transfer coefficient value of 75 $W/m^{2o}C$ being applied over all external surfaces. As shown in Figure 14, several geometric variants were investigated, however, only a selected result will be presented, as shown in Figures 15 and 16, which will depict the initial and final optimised design schemes as finite element meshes and the zones of liquid, mushy and solid

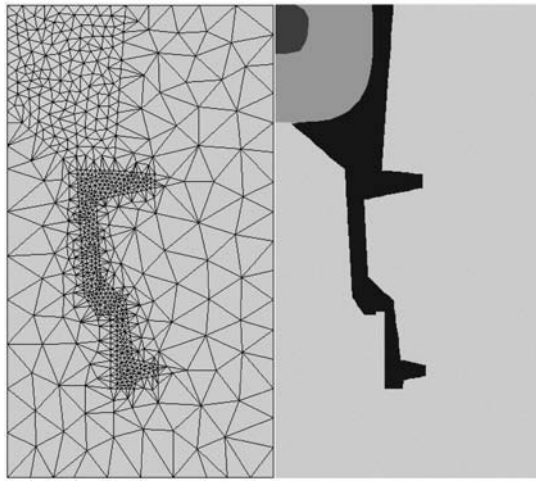

Figure 15.
Initial casting design scheme (cooling time = 3 s)

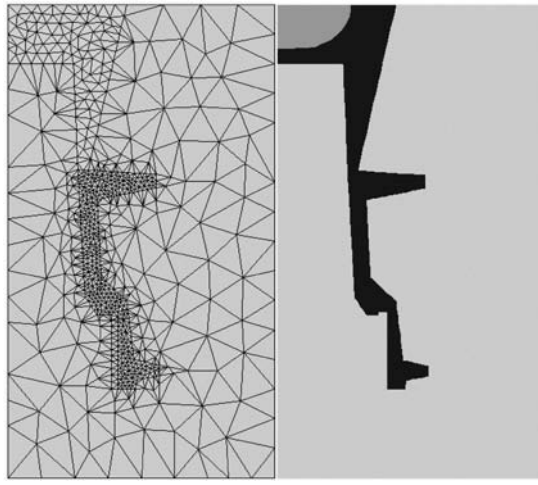

Figure 16.
Final optimised casting design scheme (cooling time = 3 s)

materials. Clearly, the initial result is a feasible casting since the last zone to solidify lies in the feeder system. However, the feeder is large in comparison with the casting and represents a significant energy waste since the metal is recycled in its molten form.

The final design shows a much reduced size of the feeder system, which still gives an acceptable part with a mushy zone left only in the feeder with an elapsed time of 3 s, thus highlighting the reduction in cycle time for the optimum design. From a practical viewpoint, trials in the foundry confirmed the benefit of the feeder size reduction as highlighted in Figures 15 and 16.

5. Meshless methods – an alternative technique for mould filling simulation

In recent years, a family of meshless methods have been developed to solve large deformation problems in both fluid and solid mechanics to maximize the advantage of Langrangian numerical simulations. These meshless methods do not need meshes or grids in their formulation. Since these particle methods involve only a number of nodal points, or particles, they are totally free from mesh entanglement and distortion, which may occur in the computational simulation of large deformation problems using traditional mesh-based methods. Hence, the advent of mesh-free methods has led to the opening of new avenues in the numerical computational field. Consequently, particle-based methods have emerged as an attractive alternative for modelling mould filling simulation in casting processes. In this section, the Corrected Smooth Particle Hydrodynamics (CSPH) method (Bonet and Kulasegaram, 2000; Bonet and Lok, 1999) was used to simulate mould filling of a gravity die casting problem similar to that given by Sirrell *et al.* (1996). CSPH is a Lagrangian method based on smooth particle hydrodynamics (SPH) (Bonet and Kulasegaram, 2000; Bonet and Lok, 1999; Lucy, 1977; Monaghan, 1998) techniques. In the CSPH method, the quantities determining the flow are localised on a set of particles, which move with the flow. This enables the method to easily follow complex free surfaces, including break up of the fluid into fragments.

5.1 Numerical methodology

In the SPH method, a given function $f(\mathbf{x})$ and its gradient $\nabla f(\mathbf{x})$ are approximated in terms of values of the function at a number of neighbouring particles and a kernel function $W(\mathbf{x} - \mathbf{x}_b, h) = W(\mathbf{x}, h_b)$ as,

$$f_h(\mathbf{x}) = \sum_{b=1}^{M} V_b f_b W_b(\mathbf{x}, h_b) \quad \text{and} \quad \nabla f_h(\mathbf{x}) = \sum_{b=1}^{M} f_b \mathbf{g}_b(\mathbf{x}) \tag{11}$$

where h is the smoothing length and determines the support of the kernel (Figure 17); V_b denotes a tributary volume associated with particle b (typically evaluated as the particle mass divided by the density); and in the standard SPH

technique, the gradient vector $\mathbf{g}$ is simply $\mathbf{g}_b = V_b \nabla W_b$. However, in CSPH methods gradient functions are amended to ensure that the gradient of general constant or linear function is correctly evaluated. This requirement leads to two simple conditions for these gradient vectors, namely:

$$\sum_{b=1}^{M} \mathbf{g}_b(\mathbf{x}) = 0 \quad \text{and} \quad \sum_{b=1}^{M} \mathbf{x} \otimes \mathbf{g}_b(\mathbf{x}) = \boldsymbol{I} \tag{12}$$

A detailed description of various methodologies that can be adopted to fulfil the above conditions can be found in the literature (Bonet and Kulasegaram, 2000; Bonet and Lok, 1999). The formulation of governing equations for mould filling simulation is described in the following section. Detailed discussions on the derivations of governing equations can be found in the literature (Kulasegaram *et al.*, 2002; Kulasegaram *et al.*, 2003).

5.2 Equations of motion

Now consider a continuum represented by a large set of Lagrangian particles as shown in Figure 18. Each particle a is described by a mass m_a, position vector $\mathbf{x}_a$ and velocity v_a.

The equations of motion can be expressed in variational or energy form by defining the total kinetic energy K, total internal energy Π_{int} and total external energy Π_{ext} as;

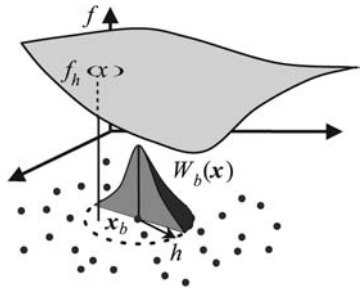

Figure 17.
SPH interpolation

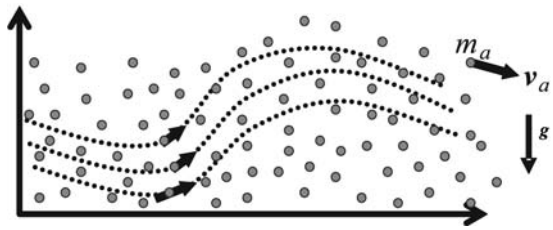

Figure 18.
Representation of continuum by a set of particles

$$K = \frac{1}{2}\sum_a m_a(v_a \cdot v_a); \quad \Pi_{\text{int}} = \sum_a m_a \pi(\rho, \ldots);$$
$$\Pi_{\text{ext}} = -\sum_a m_a(\mathbf{x}_a \cdot \mathbf{g}) \tag{13}$$

where π will depend on the deformation, density or other constitutive parameters and $\mathbf{g}$ represents the gravitational field. The equations of motion of the system of particles representing the continuum can now be evaluated following the classical Lagrangian formalism to give:

$$\frac{\mathrm{d}}{\mathrm{d}t}\left(\frac{\partial L}{\partial \mathbf{v}_a}\right) - \left(\frac{\partial L}{\partial \mathbf{x}_a}\right) = 0; \quad L(\mathbf{x}_a, \mathbf{v}_a) = K(\mathbf{v}_a) - \Pi_{\text{int}}(\mathbf{x}_a) - \Pi_{\text{ext}}(\mathbf{x}_a) \tag{14}$$

Substituting equations (13) into the above expressions leads to the standard Newton's second law for each particle as:

$$m_a \mathbf{a}_a = \mathbf{F}_a - \mathbf{T}_a \tag{15}$$

where the external $\mathbf{F}_a$ and internal $\mathbf{T}_a$ forces are;

$$\mathbf{F}_a = -\frac{\partial \Pi_{\text{ext}}}{\partial \mathbf{x}_a} = m_a \mathbf{g}; \quad \mathbf{T}_a = \frac{\partial \Pi_{\text{int}}}{\partial \mathbf{x}_a} = \frac{\partial}{\partial \mathbf{x}_a}\sum_b m_b \pi\,(\rho_b, \ldots) \tag{16}$$

The evaluation of the internal forces will depend on constitutive definition of the material. For incompressible fluid by using equation (11) to evaluate the density, an expression for internal force can be obtained as:

$$\mathbf{T}_a = \sum_b m_a m_b \left(\frac{p_a}{\rho_a^2} + \frac{p_b}{\rho_b^2}\right)\nabla W(\mathbf{x}_a)_b; \quad p = \rho^2 \frac{\mathrm{d}\pi}{\mathrm{d}\rho} \tag{17}$$

where pressure p is related as shown above to the internal energy.

In the context of the proposed variational formulation, viscosity can be introduced via dissipative potential. This leads to a new term in the Lagrange equations as,

$$\frac{\mathrm{d}}{\mathrm{d}t}\left(\frac{\partial L}{\partial \mathbf{v}_a}\right) - \left(\frac{\partial L}{\partial \mathbf{x}_a}\right) = -\frac{\partial \Pi_{\text{dis}}}{\partial \mathbf{v}_a}. \tag{18}$$

In general, the dissipative potentials are expressed as the sum of the viscous potentials per unit mass ψ, which in turn are functions of the rate of deformation tensor $\mathbf{d}$, as,

$$\Pi_{\text{dis}} = \sum_a m_a \psi(\mathbf{d}); \quad 2\mathbf{d} = \nabla v + \nabla v^{\mathrm{T}}. \tag{19}$$

For instance, in the case of a Newtonian fluid, the viscous stresses are defined by:

$$\sigma^{\text{vis}} = 2\mu \mathbf{d}'; \quad \mathbf{d}' = \mathbf{d} - \frac{1}{3}(\text{tr}\,\mathbf{d})\boldsymbol{I} \tag{20}$$

where μ is the material viscosity and $\mathbf{d}'$ is the deviatoric rate of the deformation tensor. The gradient of the velocity at each cotinuum particle is obtained with the help of equation (11) as,

$$\nabla \mathbf{v}_a = \sum_{b=1}^{M_a} \mathbf{v}_b \otimes \mathbf{g}_b(\mathbf{x}_a). \tag{21}$$

After some algebraic manipulation the internal forces due to viscous effects can be evaluated as,

$$T_a^{\text{vis}} = \frac{\partial \Pi_{\text{dis}}}{\partial \mathbf{v}_a} = \sum_b m_b \left(\frac{\sigma_b^{\text{vis}}}{\rho_b} \right) \mathbf{g}_a(\mathbf{x}_b). \tag{22}$$

Thermal effects associated with the dynamics of the material can also be easily incorporated with the above equations to simulate the gravity die casting process. The velocities and positions of the particles are updated by an explicit leap-frog time integration scheme defined by,

$$\mathbf{v}_a^{n+\frac{1}{2}} = \mathbf{v}_a^{n-\frac{1}{2}} + \Delta t \mathbf{a}_a^n; \quad \mathbf{x}_a^{n+\frac{1}{2}} = \mathbf{x}_a^n + \Delta t \mathbf{v}_a^n \tag{23}$$

The following example compares the flow patterns given by the meshless method with a solution given by the finite element method. An input velocity of 3.5 m/s has been considered for this gravity die casting benchmark geometry. The major disadvantage of the meshless method is that it is computationally very expensive as compared to an equivalent finite element analysis. This is due to the fact that in the case of meshless method searching of neighbouring particle as well as the searching of particle closer to the boundaries have to be performed at every time step. In addition, using explicit type time stepping scheme also enforces the restriction on maximum size of the time step. However, this research has shown that the method compares well with the finite element method and has a potential advantage in simulating flow through pressure die casting process where jetting and splashing effect is predominant and where the finite element method suffers from meshing difficulties. Figure 19 shows some of the initial results of this comparison.

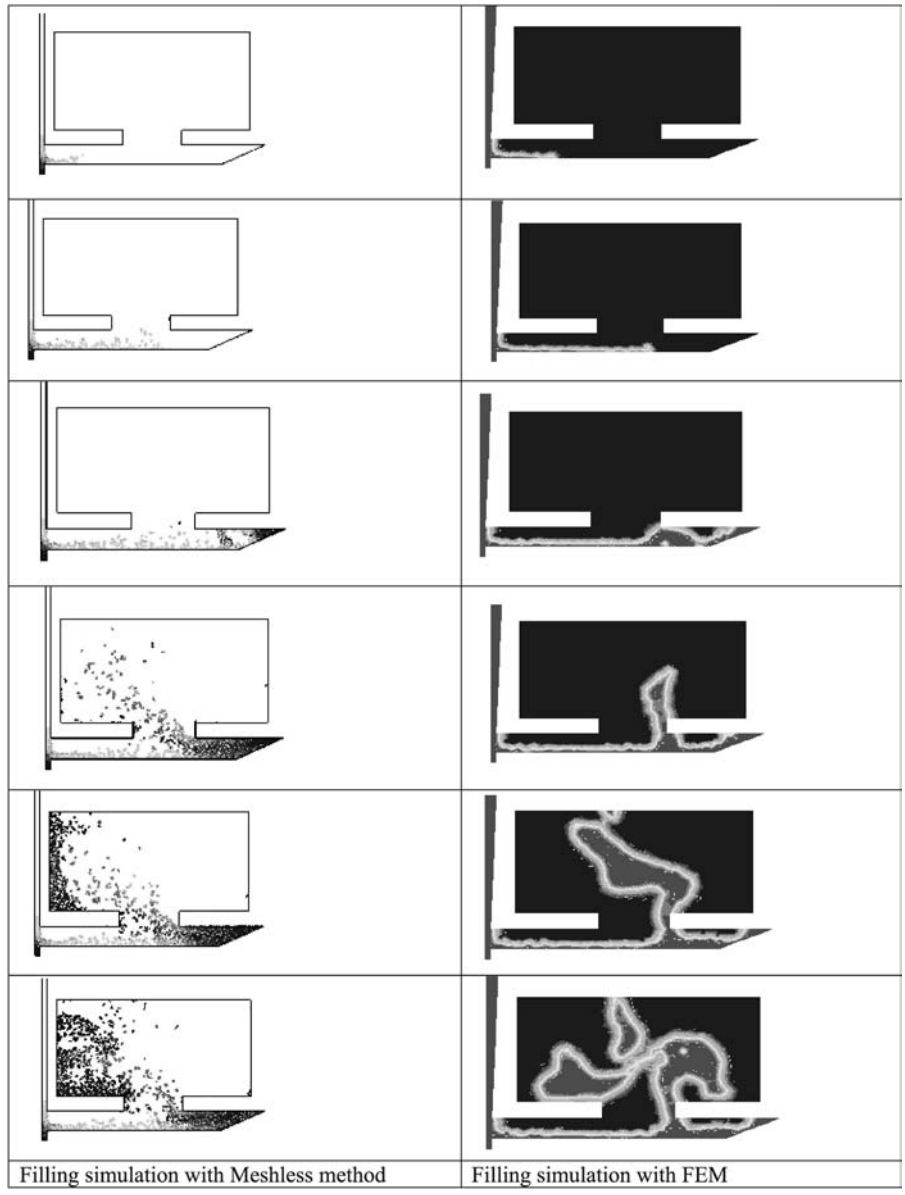

Figure 19.
Comparison of the mould filling simulation pattern between the meshless method and finite element method

6. Conclusions

The paper proposes some alternative methods for casting simulation in order to overcome some of the limitations of the finite element method. One of the major advantages of using numerical simulation tools for the casting process is to avoid expensive experimental trials in choosing optimal process, material and

design parameters. As illustrated in this paper, finite element based thermal optimisation of castings offers a way forward to assist optimal feeding of castings. However, this procedure is computationally expensive. A novel method of interpolating one-dimensional finite element solutions using the MAT technique has been demonstrated in this paper to predict the solidification pattern. The main advantage of this method was the reduction in the computational costs which may make the optimisation process computationally economical and hence feasible in a foundry environment.

In the later part of the paper, another limitation of the finite element simulation is addressed. Splashing and jetting effects are common during the mould filling process and are particularly important for the pressure die casting process. The free surface modelling of this phenomenon is a complex problem and is associated with the problems of mesh distortion and entanglement. An alternative technique, based on a meshless method, has been explored in this paper and results are compared with the finite element method. The meshless method seems to be more accurate for capturing free surface flow, however, at this stage it appears to be more computationally expensive.

References

Barlow, J. and Davis, G.A.O. (1986), "Selected FE benchmarks in structural and thermal analysis", Technical Report FEBSTA REV 1, NAFEMS.

Bletzinger, K-U., Reitinger, R., Kimmich, S. and Ramm, E. (1992), "Shape optimisation with program CARAT; software systems for structural optimisation", *International Series of Numerical Mathematics*, Vol. 110, pp. 97-124.

Blum and Harry (1967), *A Transformation for Extracting New Descriptors of Shape. Models for the Perception of Speech and Visual Form*, Whaten-Dunn, W. (Ed.), MIT Press, Cambridge, MA, pp. 362-80.

Bonet, J. and Kulasegaram, S. (2000), "Correction and stabilization of smooth particle hydrodynamics method with applications in metal forming simulations", *Int. J. Num. Meth. Eng.*, Vol. 47, pp. 1189-214.

Bonet, J. and Lok, T.S.L. (1999), "Variational and momentum aspects of smooth particle hydrodynamics formulations", *Comput. Methods. Appl. Meth. Mech. Eng.*, Vol. 180, pp. 97-115.

Carslaw, H.S. and Jaeger, J.C. (2000), *Conduction of Heat in Solids*, 2nd ed., reprinted series, Oxford Sc. Pub., Oxford, UK.

Chandrupatla, T.R. and Belegundu, A.D. (1991), *Introduction to Finite Elements in Engineering*, Prentice-Hall International Editions, Englewood Cliffs, NY.

DOT User Manual (1985), 4.20 Vanderplaats R&D inc.

Evans, G., Middleditch, A. and Miles, N. (1998), "Stable computation of the 2D medial axis transform", *Int. J. Comp. Geom. & Application*, Vol. 8 No. 5, pp. 577-98.

Gursoy, H.N. and Patrikalakis, N.M. (1991), "Automated interrogation and adaptive subdivision of shape using the medial axis transform", *Adv. Eng. Soft.*, Vol. 13, pp. 287-302.

Hinton, E., Rao, N.V.R. and Seinz, J. (1992), "Finite element structural shape and thickness optimisation of axisymmetric shells", *Engineering Computations*, Vol. 9, pp. 499-527.

Kulasegaram, S., Bonet, J., Lewis, R.W. and Profit, M. (2002), "Mould filling simulation in high pressure die casting by meshless method", *WCCM V*, Vienna.

Kulasegaram, S., Bonet, J., Lewis, R.W. and Profit, M. "High pressure die casting simulation using a Lagrangian particle method", *Communications in Numerical Methods in Engineering* (in press).

Lewis, R.W. and Ransing, R.S. (1998), "A correlation to describe interfacial heat transfer coefficients during solidification simulation and its use in the optimal feeding design of castings", *Metallurgical and Materials Transactions-B*, Vol. 29B No. 2, pp. 437-48.

Lewis, R.W., Morgan, K., Thomas, H.R. and Seetharamu, K.N. (1997), *The Finite Element Method in Heat Transfer Analysis*, Wiley, Chichester, England.

Lucy, L.B. (1977), "A numerical approach to the testing of fusion process", *The Astronomical J.*, Vol. 82, pp. 1013-24.

Monaghan, J.J. (1998), "An Introduction to SPH", *Comput. Phys. Commun.*, Vol. 48, pp. 89-96.

Morthland, T.E., Byrne, B.E., Tortorelli, D.A. and Danzig, J.A. (1995), "Optimal riser design for metal castings", *Metallurgical and Materials Transactions B*, Vol. 26B No. 4, pp. 871-85.

Pao, W.K.S., Ransing, R.S., Lewis, R.W. and Lin, C. (2002), "Solidification prediction in casting design using medial-axes-based interpolation technique", *Finite Element Analy. & Design*, (accepted for publication).

Sheehy, D.J., Armstrong, C.G. and Robinson, D.J. (1996), "Shape description by medial surface construction", *IEEE Transaction on Visualization and Computer Graphics*, Vol. 2 No. 1, pp. 62-72.

Sirrell, B., Holliday, M. and Campbell, J. (1996), "Benchmark testing the flow and solidification modelling of Al castings", *J. of Mat.*, pp. 20-3.

Tam, T. and Armstrong, C.G. (1991), "2D finite element mesh generation by medial axis subdivision", *Adv. Eng. Soft.*, Vol. 13, pp. 312-24.

Vanderplaats, G.N. (1984), *Numerical Optimisation Techniques for Engineering Design – With Applications*, McGraw-Hill, New York, NY.

Further reading

Libersky, L.D., Petschek, A.G., Carney, T.C., Hipp, J.R. and Allahadi, F.A. (1993), "High strain Lagrangian hydrodynamics", *J. Comput. Phys.*, Vol. 109, pp. 67-75.